










**Control of perpendicular magnetic anisotropy at the Fe/MgO interface by phthalocyanine insertion**Shoya Sakamoto <sup>1</sup>, Edward Jackson <sup>2</sup>, Takeshi Kawabe,<sup>3</sup> Takuya Tsukahara <sup>3</sup>, Yoshinori Kotani <sup>4</sup>, Kentaro Toyoki,<sup>4</sup> Emi Minamitani <sup>5</sup>, Yoshio Miura <sup>6</sup>, Tetsuya Nakamura <sup>4</sup>, Atsufumi Hirohata <sup>2</sup>, and Shinji Miwa <sup>1,3,7,\*</sup><sup>1</sup>*The Institute for Solid State Physics, The University of Tokyo, Chiba 277-8581, Japan*<sup>2</sup>*Department of Electronic Engineering, University of York, York YO10 5DD, United Kingdom*<sup>3</sup>*Graduate School of Engineering Science, Osaka University, Osaka 560-8531, Japan*<sup>4</sup>*Japan Synchrotron Radiation Research Institute (JASRI), Hyogo 679-5198, Japan*<sup>5</sup>*Department of Theoretical and Computational Molecular Science, Institute for Molecular Science, Aichi 444-8585, Japan*<sup>6</sup>*National Institute for Materials Science (NIMS), Ibaraki 305-0047, Japan*<sup>7</sup>*Trans-scale Quantum Science Institute, The University of Tokyo, Bunkyo, Tokyo 113-0033, Japan*

(Received 7 January 2022; revised 11 April 2022; accepted 19 April 2022; published 13 May 2022)

Perpendicular magnetic anisotropy at an interface between Fe and MgO with Co-phthalocyanine (CoPc) adsorption has been investigated. We find that the CoPc adsorption at an Fe/MgO interface increases the perpendicular magnetic anisotropy energy (PMA) while maintaining the voltage-controlled magnetic anisotropy effect. By performing x-ray magnetic circular dichroism spectroscopy measurements, we reveal that the CoPc adsorption induces hole accumulation at the Fe surface. The origin of the PMA enhancement is attributed to the increased orbital magnetic moment anisotropy of the Fe atoms.

DOI: [10.1103/PhysRevB.105.184414](https://doi.org/10.1103/PhysRevB.105.184414)**I. INTRODUCTION**

Perpendicular magnetic anisotropy (PMA) in ultrathin ferromagnetic metals has been intensively studied [1–7]. This is partially because it is applicable for high-density magnetic recording disks and magnetic random-access memory (MRAM) devices. Moreover, the control of the PMA energy by an external voltage, or the voltage-controlled magnetic anisotropy (VCMA) effect, has attracted significant attention due to its potential for an energy-efficient operation technology of MRAM [6–13]. The PMA in such ultrathin films has often been studied for heterostructures with heavy metals (cf. Co/Pd, Co/Pt, Co/Au) and oxides [cf. Co/AlO<sub>x</sub>, Fe/MgO, Fe(CoB)/MgO] [6]. The interfacial orbital hybridization between a ferromagnet and a heavy metal (or oxide) often induces the magnetization direction dependence of the orbital magnetic moment, which is one of the main origins of PMA [2–4].

In addition to interfaces with heavy metals or oxides, molecule adsorption on the surface of ferromagnetic metals may change the PMA energy in a similar manner. For instance, it has been reported that the Au(111)/Co(0001)/C<sub>60</sub> multilayer shows larger PMA energy than that of Au(111)/Co(0001)/vacuum by  $\sim 0.25$  mJ/m<sup>2</sup> [14]. The PMA enhancement is attributed to hybridization between Co *d*<sub>z<sup>2</sup></sub> orbitals and the C atoms of C<sub>60</sub>. Despite this promising finding, PMA in other ferromagnet-molecule interfaces remains largely uninvestigated. Moreover, the feasibility of the VCMA effect at metal-molecule interfaces is an open question.

Recently, an epitaxial-like metal-molecule multilayer was reported using phthalocyanine (Pc) molecules, and magnetic tunneling junction (MTJ) devices with the Fe(001)/CoPc/MgO(001) multilayer showed a sizable tunneling magnetoresistance ratio of  $\sim 20\%$  [15]. Such a device is suitable for investigating PMA and VCMA effect at metal-molecule interfaces. In this paper, we study PMA and VCMA effect in Fe(001)/CoPc/MgO(001)-based MTJ devices by performing spin-torque ferromagnetic resonance (STFMR) and x-ray magnetic circular dichroism (XMCD) spectroscopy measurements. From the STFMR measurements, we found that the PMA is enhanced while maintaining the VCMA. The origin of the enhancement of PMA is related to the hole accumulation of the Fe surface, which is supported by the XMCD measurements and *ab initio* calculation.

**II. METHODS**

Figure 1(a) shows a schematic of the film structure. The film was grown by molecular beam epitaxy under ultrahigh vacuum. First, an MgO(001) substrate was annealed at 800 °C for 10 min. Then, MgO(001) (5 nm)/V(001) (30 nm) buffer layers were deposited at room temperature and subsequently annealed at 500 °C for 15 min. After that, Fe, CoPc, MgO barrier, Fe (10 nm), and Au (5 nm) layers were grown at room temperature. CoPc was deposited using an effusion cell, and other materials were deposited using an electron-beam gun [15].

For the transmission electron microscope (TEM) measurements (Fig. 1), an Fe(0.5 nm)/CoPc(0.32 nm, 3.2 nm)/MgO(1.7 nm) continuous multilayer was employed. For the STFMR measurements (Fig. 2), a stack with Fe(0.4 nm)/CoPc/MgO(1.4 nm) was patterned into MTJ

\*miwa@issp.u-tokyo.ac.jp

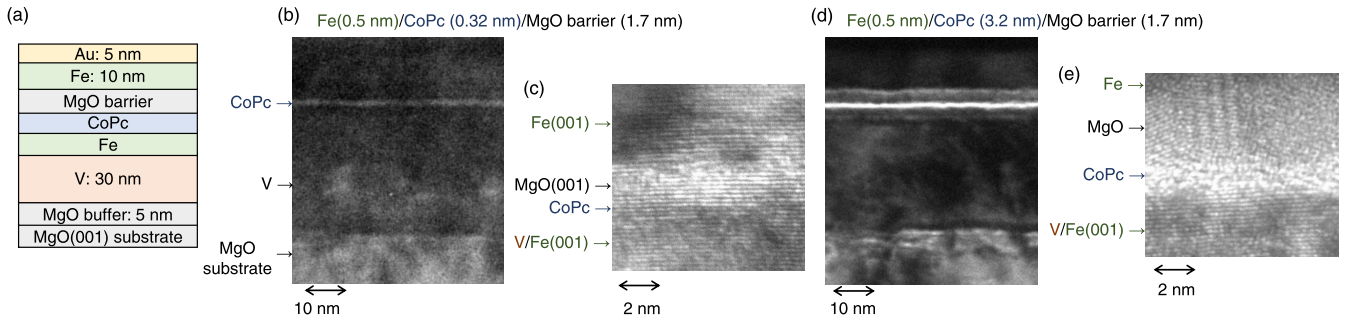


FIG. 1. (a) Schematic of the film stack. (b),(c) Transmission electron microscope (TEM) images of the multilayers with 0.32 nm thick CoPc layer. (d),(e) TEM images of the multilayer with 3.2 nm thick CoPc layer.

devices with an area of  $2 \times 5 \mu\text{m}^2$  by the combination of photolithography, Ar-ion milling, and lift-off methods. Here, a slightly thin Fe layer of 0.4 nm was employed to optimize the total PMA energy to increase the signal to noise ratio in the STFMR measurements. For the XMCD spectroscopy measurements (Figs. 3 and 4), an Fe(0.5 nm)/CoPc(0–0.35 nm)/MgO(2 nm) multilayer without Fe/Au capping layers was employed. The XMCD spectroscopy measurements were conducted at the soft x-ray beamline BL25SU of SPring-8 [16,17]. The x-ray absorption signals were recorded with circularly polarized x rays with right ( $\mu_+$ ) and left ( $\mu_-$ ) helicities at room temperature using the total electron yield method.

To support the experimental results, *ab initio* calculations were carried out using the Vienna *ab initio* simulation package [18,19]. We performed spin-polarized calculations using the generalized gradient approximation (GGA) with the Perdew-Burke-Ernzerhof functional [20] and projector augmented

wave pseudopotentials [21,22]. The cutoff energy of the plane-wave basis set was 400 eV. The interface between CoPc and Fe was described by a slab model consisting of five atomic layers of Fe (100) with  $5 \times 5$  periodicity adsorbed by one CoPc molecule. In other words, approximately 25 Fe atoms are directly interfaced with one CoPc molecule. The surface Brillouin zone was sampled on the Gamma centered mesh of  $3 \times 3$ . The convergence criteria for the self-consistent field calculations and structure optimization were  $5.0 \times 10^{-6}$  eV and  $0.02 \text{ eV/\AA}$ , respectively. The PMA energy was estimated by comparing the total energies including the spin-orbit coupling with the different magnetization directions ([100] and [001]).

### III. RESULTS AND DISCUSSION

Figure 1 shows the TEM images captured for the multilayer stack: MgO substrate/MgO buffer (5 nm)/V

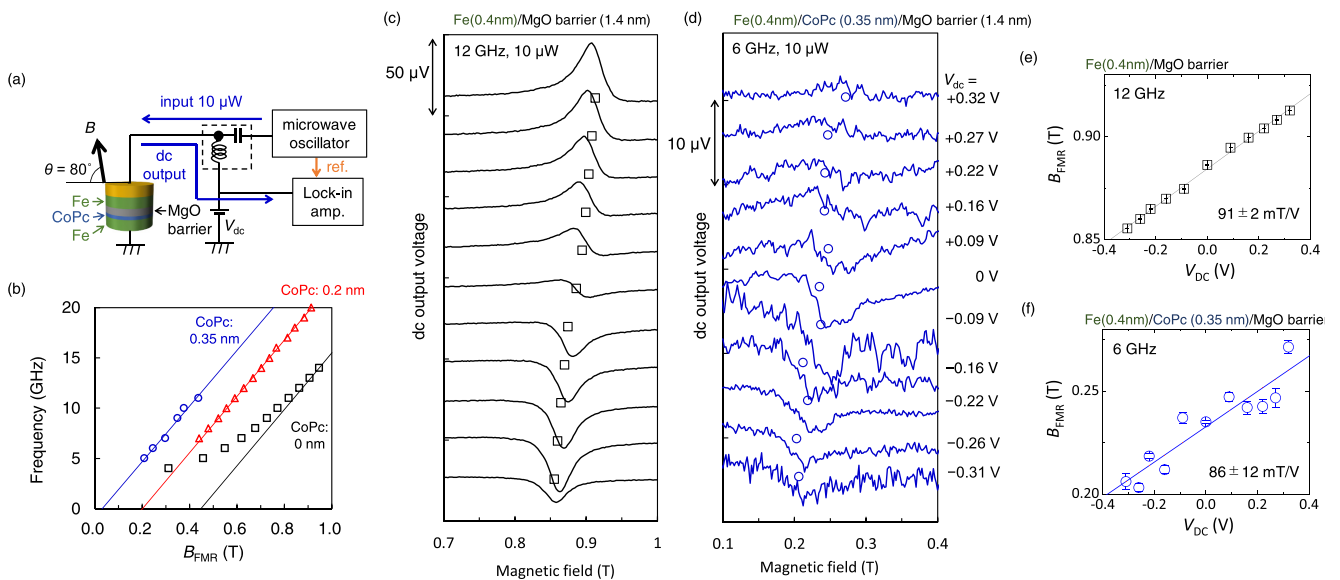


FIG. 2. (a) Schematic illustration of the measurement setup for the spin-torque ferromagnetic resonance (STFMR) with voltage-driven torque. (b) Input microwave frequency as a function of the resonant magnetic field. (c) STFMR spectra for a magnetic tunnel junction without CoPc layer [Fe(0.4 nm)/MgO]. The black squares show resonant field for each spectrum. (d) STFMR spectra for a magnetic tunnel junction with 0.35 nm CoPc layer [Fe(0.4 nm)/CoPc(0.35 nm)/MgO]. The blue circles show resonant field for each spectrum. (e) Voltage-induced changes of the resonant magnetic field in an Fe/MgO device. (f) Voltage-induced changes of the resonant magnetic field in an Fe/CoPc(0.35 nm)/MgO device.

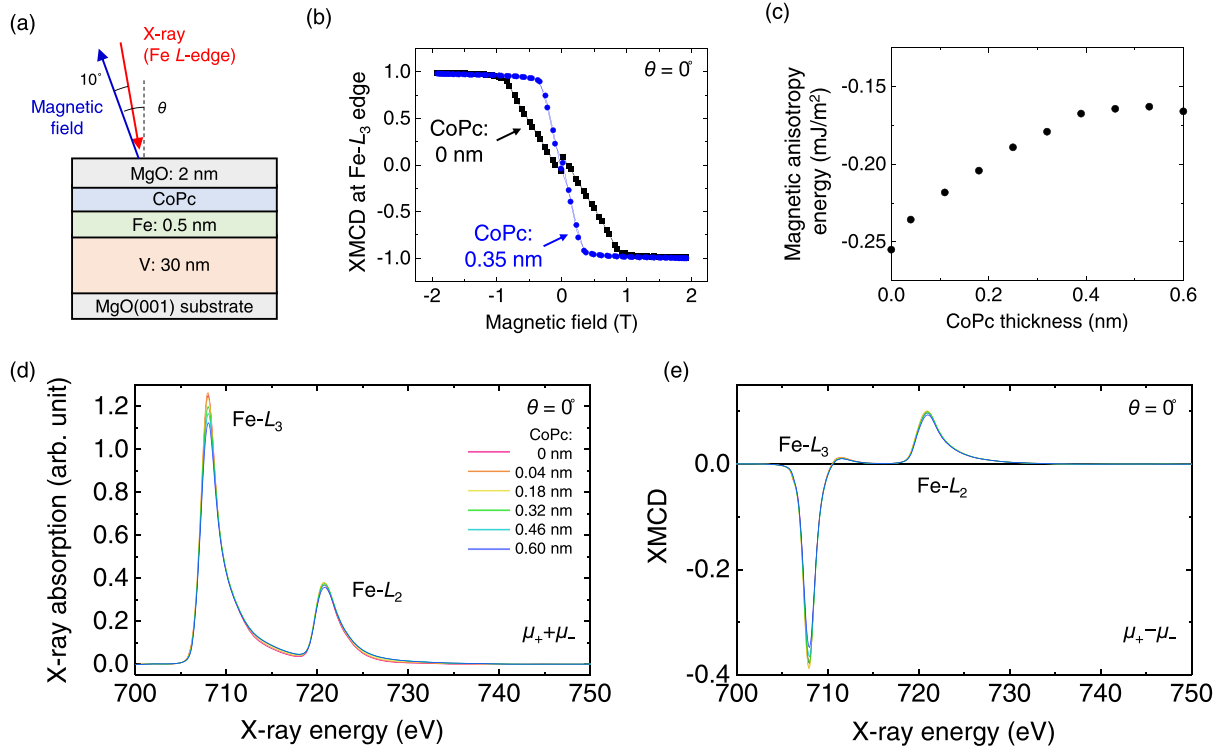


FIG. 3. (a) Schematic illustration of the measurement setup for x-ray magnetic circular dichroism (XMCD) spectroscopy with the total electron yield method. (b) Magnetization hysteresis curves taken by measuring Fe- $L_3$  edge XMCD signals. (d) Fe- $L_{2,3}$  edge x-ray absorption spectra and (e) XMCD spectra under a magnetic field of 1.9 T with the perpendicular ( $\theta = 0^\circ$ ) configuration.

(30 nm)/Fe(0.5 nm)/CoPc (0.32 nm, 3.2 nm)/MgO barrier (1.7 nm)/Fe(10 nm)/Au(5 nm). Figures 1(b) and 1(c) show the results for 0.32 nm thick CoPc. The 0.32 nm thick CoPc almost corresponds to one molecular layer of CoPc. From Fig. 1(c), we can see that the MgO and Fe layers were epitaxially grown on Fe/CoPc(0.32 nm). Figures 1(d) and 1(e)

show the results for 3.2-nm-thick CoPc (ten molecular layers of CoPc). Contrary to the case of 0.32 nm thick CoPc, the MgO and Fe layers on Fe/CoPc(3.2 nm) are polycrystalline, as can be seen in Fig. 1(e). Previous reflection high-energy electron diffraction experiments revealed that MgO(001) can be epitaxially grown on Fe/CoPc when the CoPc nominal thickness is less than two molecular layers ( $\sim 0.7$  nm) [15], and the present TEM results are consistent with this previous study. Note that epitaxial Fe(001)/CoPc(0.32 nm)/MgO(001) was employed for the STFMR and XMCD measurements.

Figure 2 shows the results of the STFMR measurements with voltage-driven torque [23,24]. For these measurements, the multilayer stack of MgO substrate/MgO (5 nm)/V (30 nm)/Fe(0.4 nm)/CoPc (0–0.35 nm)/MgO (1.4 nm)/Fe(10 nm)/Au(5 nm) was patterned into MTJ devices. Figure 2(a) shows a schematic of the measurement circuit. A microwave power of 10  $\mu$ W was applied through a bias tee to the MTJ device, and the dc output voltage generated in the MTJ was measured with a lock-in amplifier. The STFMR spectra were recorded by sweeping a magnetic field in the direction of  $\theta = 80^\circ$  from the film surface. Figure 2(b) shows the resonant magnetic field as a function of the input microwave frequency. With this nearly normal direction of the magnetic field ( $\theta = 80^\circ$ ), the intercept of the linear fit almost corresponds to the saturation magnetic field in the perpendicular direction [7]. We can see that the saturation magnetic field decreases when the CoPc nominal thickness increases. This means that the PMA was enhanced by the CoPc adsorption.

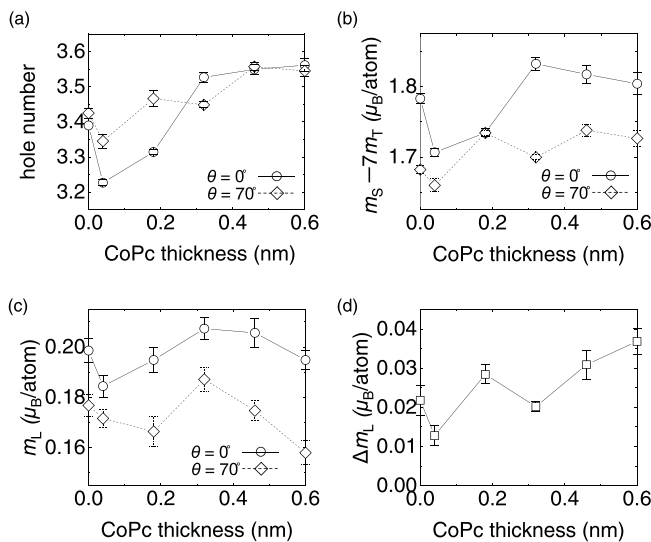


FIG. 4. (a) Hole number, (b) effective spin magnetic moment, (c) orbital magnetic moment of the Fe atoms, and (d) orbital magnetic moment anisotropy of the Fe atoms.

The increase of the PMA energy by the molecular adsorption is similar to the case of Co(111)/C<sub>60</sub> and opposite to the case of Fe(110)/C<sub>60</sub> [14].

Figures 2(c) and 2(d) show the STFMR spectra under various dc bias voltages ( $V_{dc}$ ) to characterize the VCMA effect. Here, the VCMA effect should be characterized where the linear relationship between the input microwave frequency and the resonant magnetic field is satisfied as shown in Fig. 2(b). Therefore a relatively large microwave frequency of 12 GHz was employed for the Fe/MgO to satisfy the condition. For the Fe/CoPc/MgO, while almost all of the data were in the linear region, we have employed the relatively low frequency of 6 GHz to improve the signal to noise ratio. When the dc bias voltage is not applied ( $V_{dc} = 0$  V), the STFMR spectrum has an anti-Lorentzian shape. This anti-Lorentzian structure is typical for STFMR spectra driven by the VCMA effect [23,24]. This is because the Lorentzian (anti-Lorentzian) structure represents the STFMR signals driven by in-plane (perpendicular) spin torque, and the voltage-driven torque originating from the VCMA effect is a perpendicular torque. As the dc bias voltage magnitude increases, the spectral line shapes change from an anti-Lorentzian-like to a Lorentzian-like structure. This change in the spectral line shape originates from the nonlinear spin-torque diode effect [25,26]. Under the dc bias voltage, the STFMR spectra originating from the second-order precession angle may dominate. Because such second-order STFMR is not phase sensitive to the input microwave, the spectral line shape becomes Lorentzian.

To characterize the resonant magnetic field, the obtained spectra were fitted by the equation including both Lorentzian ( $(\Delta B)^2 / [(B - B_{FMR})^2 + (\Delta B)^2]$ ) and anti-Lorentzian ( $(\Delta B)^2 (B - B_{FMR}) / [(B - B_{FMR})^2 + (\Delta B)^2] (\Delta B)^2$ ) functions. Here,  $B$ ,  $B_{FMR}$ , and  $\Delta B$  are the external magnetic field, resonant magnetic field, and spectral linewidth, respectively. The black squares in Fig. 2(c) and blue circles in Fig. 2(d) show the resonant fields for Fe/MgO and Fe/CoPc(0.35 nm)/MgO, respectively. As shown in Figs. 2(c) and 2(d), the resonant magnetic field increases as the dc bias voltage increases. The resonant magnetic field as a function of the dc bias voltage for the Fe/MgO and Fe/CoPc/MgO MTJs are plotted in Figs. 2(e) and 2(f), respectively. The voltage-induced changes in the resonant magnetic field, which directly reflect the VCMA effect, are almost equivalent to each other ( $91 \pm 2$  mT/V for Fe/MgO and  $86 \pm 12$  mT/V for Fe/CoPc/MgO). Here, 91 mT/V for Fe/MgO corresponds to the VCMA coefficient of 36 fJ/V m. This STFMR study demonstrates that the CoPc adsorption at the Fe/MgO interface enlarges the PMA energy while maintaining the VCMA effect.

To further investigate the PMA enhancement by the CoPc adsorption, XMCD spectroscopy measurements were conducted on the multilayer stack: MgO substrate/MgO (5 nm)/V (30 nm)/Fe(0.5 nm)/CoPc (0–0.6 nm)/MgO (2 nm) [Fig. 3(a)]. Figure 3(b) shows the hysteresis curves for the multilayers with (CoPc: 0.35 nm) and without (CoPc: 0 nm) a CoPc layer at the Fe/MgO interface. The hysteresis curves were taken by measuring the Fe- $L_3$  edge XMCD signals. From Fig. 3(b), the saturation magnetic field in the perpendicular direction is found reduced by the CoPc adsorption. This PMA

enhancement is consistent with the STFMR results shown in Fig. 2(b). From the magnetization hysteresis curves, PMA energies for various CoPc thicknesses are quantitatively estimated, as shown in Fig. 3(c). The PMA energy monotonically increases and saturates around 0.4 nm. Here, the saturation of the PMA energy seems to coincide with the one molecular layer coverage.

The x-ray absorption  $[(\mu_+ + \mu_-)/2]$  and XMCD  $(\mu_+ - \mu_-)$  spectra are displayed in Figs. 3(d) and 3(e), respectively. A magnetic field of  $\pm 1.9$  T was applied to saturate the magnetization of the Fe layer. The background consisting of a double step function and a linear function that bends at the Fe- $L_3$  edge [27] is subtracted from the raw data. The spectra are normalized by the height of the edge jump at the Fe- $L$  edge. As can be seen in Fig. 3(d), the CoPc adsorption broadened the spectra slightly: It reduced a peak height at the Fe- $L_3$  edge ( $\sim 708$  eV) and slightly increased the baseline around 715 eV. Note that the change in the x-ray absorption spectra differs from that observed in Fe oxides, where a distinct shoulder appears around 709 eV [28].

From the x-ray absorption and XMCD spectra, a hole number of the Fe 3d orbitals, effective spin magnetic moment, and orbital magnetic moment are derived, as shown in Fig. 4. To estimate errors associated with the arbitrariness in the spectral background subtraction process, we subtracted about a hundred different background from the spectra. The plotted data and error bars in Fig. 4 are the average values and standard deviations resulting from those background subtraction trials. Figure 4(a) shows 3d hole numbers of Fe. Here, we assume that the Fe 3d hole number in perpendicular magnetization is 3.39 [29] in the absence of CoPc and plot the relative hole number that is determined from the integrals of the x-ray absorption spectra. From Fig. 4(a), we can see that the CoPc adsorption increases the Fe 3d hole number by  $\sim 0.09$ . Figure 4(b) shows the effective spin magnetic moment ( $m_S - 7m_T$ ) [30]. The effective spin magnetic moments under both perpendicular ( $\theta = 0^\circ$ ) and in-plane ( $\theta = 70^\circ$ ) magnetic fields slightly increase by the CoPc adsorption. This almost constant spin magnetic moment confirms that the observed enhanced PMA is not due to the weakened in-plane shape magnetic anisotropy with reduced magnetization. Figure 4(c) shows the deduced orbital magnetic moments ( $m_L$ ) [31]. The anisotropy in the orbital magnetic moment ( $\Delta m_L$ ) is defined as the out of plane orbital magnetic moment subtracted by the in-plane one. The orbital magnetic moment anisotropy increases by the CoPc adsorption and saturates around 0.4–0.6 nm in the CoPc thickness, as shown in Fig. 4(d).

According to the XMCD experiments, the one molecular layer CoPc adsorption leads to a hole doping ( $\sim 0.09$ ) and increases the orbital magnetic moment anisotropy ( $\sim 0.017$ ) in the Fe 3d orbitals. As a result, the PMA energy increases by  $\sim 0.08$  mJ/m<sup>2</sup>. Given that the Fe atoms interfaced with MgO predominantly possess the orbital magnetic moment and PMA energy [5,9], the effective spin-orbit interaction coefficient ( $\lambda'$ ) in the Bruno model [2] ( $\lambda' \Delta m_L / 4\mu_B$ ) is estimated to be  $\sim 9$  meV. This value is comparable to the previous study using Cr/Fe/MgO ( $\lambda' \sim 7$  meV [32]). Therefore, the orbital magnetic moment anisotropy in the Fe 3d orbitals enhanced by the molecule adsorption seems to explain the enhanced PMA energy.

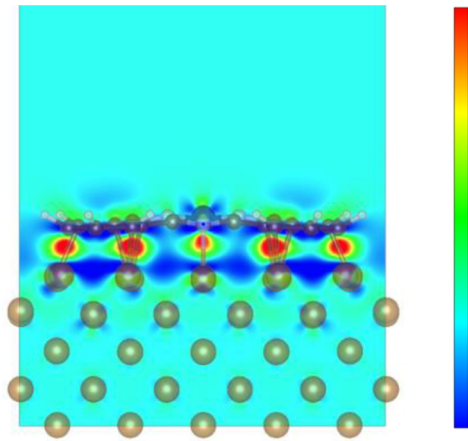


FIG. 5. Schematic of the computational model with differential charge distribution [saturated level:  $+0.06$  (red) and  $-0.02$  (blue)  $e/\text{bohr}^3$ ]. The data were visualized by VESTA [34].

The above experimental findings are supported by *ab initio* calculations. Figure 5 shows the projection of the differential charge distribution along the Fe[010] direction overlaid on the used atomic structure model. The result indicates that the interaction between Pc ligand and Fe orbitals induces charge transfer from Fe to CoPc. Indeed, comparison between the results of the Bader charge analysis [33] for isolated CoPc and Fe(001)/CoPc reveals that CoPc acquired a charge of  $3.25 e^-$  upon adsorption. This is qualitatively consistent with the hole accumulation up to eight holes per 25 Fe atoms at the Fe surface deduced from the XAS measurements. In addition, the calculations confirmed that the CoPc adsorption enhances the total PMA energy from  $0.92 \text{ mJ/m}^2$  (Fe/vacuum) to  $0.96 \text{ mJ/m}^2$  (Fe/CoPc/vacuum).

Finally, let us discuss the relation between the induced holes and the PMA energy. As described above, the VCMA coefficient of Fe/MgO was estimated to be  $36 \text{ fJ/V m}$  from Fig. 2(e). This means that a  $-1 \text{ V}$  application to the MgO barrier increases the PMA energy by  $0.025 \text{ mJ/m}^2$ . From the simple capacitance model [10], the corresponding electric field induces a hole accumulation of  $\sim 0.03$  per Fe atom at

the Fe/MgO interface, and we need a hole accumulation of 0.1 to realize the PMA enhancement of  $0.08 \text{ mJ/m}^2$  achieved by the CoPc adsorption [Fig. 3(c)]. From the x-ray absorption results shown in Fig. 4(a), one molecular layer CoPc adsorption increases the thickness-averaged Fe 3d hole number by  $\sim 0.09$ . These discussions indicate that the enhancement of the PMA energy by molecule adsorption can be qualitatively explained by the VCMA effect via adsorption-induced hole doping. In addition to this hole doping effect, hybridization between Fe 3d orbitals and C sp orbitals may also contribute to the enhanced PMA, and the effect of orbital hybridization should be investigated in future studies.

#### IV. CONCLUSION

In this paper, the PMA of the Fe/CoPc/MgO system has been studied. The CoPc adsorption at the Fe/MgO interface increases the PMA energy while the VCMA effect is almost unchanged. XMCD spectroscopy has revealed that the enhancement of the PMA energy is associated with the increase of orbital magnetic moment anisotropy and hole number in the Fe 3d orbitals. The magnitude of the orbital magnetic moment anisotropy has been found consistent with the Bruno model. Moreover, the PMA enhancement can be qualitatively explained by the VCMA effect due to the hole doping induced by the molecule adsorption. This study paves the path toward further development in the field of molecular spintronics.

#### ACKNOWLEDGMENTS

We thank M. Goto and Y. Suzuki of Osaka University, and R. Arafune of NIMS for discussion. Part of this work was supported by JSPS KAKENHI (Grants No. JP18H03880, No. JP20K15158, and No. JP22H00290) and the Spintronics Research Network of Japan (Spin-RNJ). E.J. and A.H. acknowledge the financial and technical support provided by JEOL UK. The XAS and XMCD measurements were performed in SPring-8 with the approval of the Japan Synchrotron Radiation Research Institute (Proposal No. 2017A1201). The computation was performed using the Research Center for Computational Science, Okazaki, Japan (Project No. 21-IMS-C186).

- 
- [1] P. F. Carcia, A. D. Meinhaldt, and A. Suna, Perpendicular magnetic anisotropy in Pd/Co thin film layered structures, *Appl. Phys. Lett.* **47**, 178 (1985).
  - [2] P. Bruno, Tight-binding approach to the orbital magnetic moment and magnetocrystalline anisotropy of transition-metal monolayers, *Phys. Rev. B* **39**, 865 (1989).
  - [3] G. van der Laan, Microscopic origin of magnetocrystalline anisotropy in transition metal thin films, *J. Phys.: Condens. Matter* **10**, 3239 (1998).
  - [4] J. Stöhr, Exploring the microscopic origin of magnetic anisotropies with x-ray magnetic circular dichroism (XMCD) spectroscopy, *J. Magn. Magn. Mater.* **200**, 470 (1999).
  - [5] H. X. Yang, M. Chshiev, B. Dieny, J. H. Lee, A. Manchon, and K. H. Shin, First-principles investigations of the very large perpendicular magnetic anisotropy at Fe|MgO and Co|MgO interfaces, *Phys. Rev. B* **84**, 054401 (2011).
  - [6] B. Dieny and M. Chshiev, Perpendicular magnetic anisotropy at transition metal/oxide interfaces and applications, *Rev. Mod. Phys.* **89**, 025008 (2017).
  - [7] S. Miwa, M. Suzuki, M. Tsujikawa, T. Nozaki, T. Nakamura, M. Shirai, S. Yuasa, and Y. Suzuki, Perpendicular magnetic anisotropy and its electric-field-induced change at metal-dielectric interfaces, *J. Phys. D: Appl. Phys.* **52**, 063001 (2019).
  - [8] M. Weisheit, S. Fähler, A. Marty, Y. Souche, C. Poinignon, and D. Givord, Electric field-induced modification of magnetism in thin-film ferromagnets, *Science* **315**, 349 (2007).
  - [9] C.-G. Duan, J. P. Velev, R. F. Sabirianov, Z. Zhu, J. Chu, S. S. Jaswal, and E. Y. Tsymbal, Surface Magnetoelectric Effect

- in Ferromagnetic Metal Films, *Phys. Rev. Lett.* **101**, 137201 (2008).
- [10] T. Maruyama, Y. Shiota, T. Nozaki, K. Ohta, N. Toda, M. Mizuguchi, A. Tulapurkar, T. Shinjo, M. Shiraishi, S. Mizukami, Y. Ando, and Y. Suzuki, Large voltage-induced magnetic anisotropy change in a few atomic layers of iron, *Nat. Nanotechnol.* **4**, 158 (2009).
- [11] P. K. Amiri, J. G. Alzate, X. Q. Cai, F. Ebrahimi, Q. Hu, K. Wong, C. Grèzes, H. Lee, G. Yu, X. Li, M. Akyol, Q. Shao, J. A. Katine, J. Langer, B. Ocker, and K. L. Wang, Electric-field-controlled magnetoelectric RAM: Progress, challenges, and scaling, *IEEE Trans. Magn.* **51**, 3401507 (2015).
- [12] C. Song, B. Cui, F. Li, X. Zhou, and F. Pan, Recent progress in voltage control of magnetism: Materials, mechanisms, and performance, *Prog. Mater. Sci.* **87**, 33 (2017).
- [13] T. Nozaki, T. Yamamoto, S. Miwa, M. Tsujikawa, M. Shirai, S. Yuasa, and Y. Suzuki, Recent progress in the voltage-controlled magnetic anisotropy effect and the challenges faced in developing voltage-torque MRAM, *Micromachines* **10**, 327 (2019).
- [14] K. Bairagi, A. Bellec, V. Repain, C. Chacon, Y. Girard, Y. Garreau, J. Lagoute, S. Rousset, R. Breitwieser, Y.-C. Hu, Y. C. Chao, W. W. Pai, D. Li, A. Smogunov, and C. Barretau, Tuning the Magnetic Anisotropy at a Molecule-Metal Interface, *Phys. Rev. Lett.* **114**, 247203 (2015).
- [15] T. Kawabe, K. Shimose, M. Goto, Y. Suzuki, and S. Miwa, Magnetic tunnel junction with Fe(001)/Co phthalocyanine/MgO(001) single-crystal multilayer, *Appl. Phys. Express* **11**, 013201 (2018).
- [16] T. Nakamura, T. Muro, F. Z. Guo, T. Matsushita, T. Wakita, T. Hirono, Y. Takeuchi, and K. Kobayashi, Development of a soft x-ray magnetic circular dichroism spectrometer using a 1.9 T electromagnet at BL25SU of SPring-8, *J. Electron Spectrosc. Relat. Phenom.* **144–147**, 1035 (2005).
- [17] T. Hirono, H. Kimura, T. Muro, Y. Saitoh, and T. Ishikawa, Full polarization measurement of SR emitted from twin helical undulators with use of Sc/Cr multilayers at near 400 eV, *J. Electron Spectrosc. Relat. Phenom.* **144–147**, 1097 (2005).
- [18] G. Kresse and J. Furthmüller, Efficiency of *ab-initio* total energy calculations for metals and semiconductors using a plane-wave basis set, *Comput. Mater. Sci.* **6**, 15 (1996).
- [19] G. Kresse and J. Furthmüller, Efficient iterative schemes for *ab initio* total-energy calculations using a plane-wave basis set, *Phys. Rev. B* **54**, 11169 (1996).
- [20] J. P. Perdew, K. Burke, and M. Ernzerhof, Generalized Gradient Approximation Made Simple, *Phys. Rev. Lett.* **77**, 3865 (1996).
- [21] P. E. Blöchl, Projector augmented-wave method, *Phys. Rev. B* **50**, 17953 (1994).
- [22] G. Kresse and D. Joubert, From ultrasoft pseudopotentials to the projector augmented-wave method, *Phys. Rev. B* **59**, 1758 (1999).
- [23] T. Nozaki, Y. Shiota, S. Miwa, S. Murakami, F. Bonell, S. Ishibashi, H. Kubota, K. Yakushiji, T. Saruya, A. Fukushima, S. Yuasa, T. Shinjo, and Y. Suzuki, Electric-field-induced ferromagnetic resonance excitation in an ultrathin ferromagnetic metal layer, *Nat. Phys.* **8**, 491 (2012).
- [24] J. Zhu, J. A. Katine, G. E. Rowlands, Y.-J. Chen, Z. Duan, J. G. Alzate, P. Upadhyaya, J. Langer, P. K. Amiri, K. L. Wang, and I. N. Krivorotov, Voltage-Induced Ferromagnetic Resonance in Magnetic Tunnel Junctions, *Phys. Rev. Lett.* **108**, 197203 (2012).
- [25] S. Miwa, S. Ishibashi, H. Tomita, T. Nozaki, E. Tamura, K. Ando, N. Mizuochi, T. Saruya, H. Kubota, K. Yakushiji, T. Taniguchi, H. Imamura, A. Fukushima, S. Yuasa, and Y. Suzuki, Highly sensitive nanoscale spin-torque diode, *Nat. Mater.* **13**, 50 (2014).
- [26] Y. Shiota, S. Miwa, S. Tamaru, T. Nozaki, H. Kubota, A. Fukushima, Y. Suzuki, and S. Yuasa, High-output microwave detector using voltage-induced ferromagnetic resonance, *Appl. Phys. Lett.* **105**, 192408 (2014).
- [27] S. Sakamoto, M. Tsujikawa, M. Shirai, K. Amemiya, and S. Miwa, Electron correlation enhances orbital polarization at a ferromagnetic metal/insulator interface: Depth-resolved x-ray magnetic circular dichroism and first-principles study, *ACS Appl. Electron. Mater.* **4**, 1794 (2022).
- [28] T. J. Regan, H. Ohldag, C. Stamm, F. Nolting, J. Lüning, J. Stör, and R. L. White, Chemical effects at metal/oxide interfaces studied by x-ray-absorption spectroscopy, *Phys. Rev. B* **64**, 214422 (2001).
- [29] C. T. Chen, Y. U. Idzerda, H. J. Lin, N. V. Smith, G. Meigs, E. Chaban, G. H. Ho, E. Pellegrin, and F. Sette, Experimental Confirmation of the X-Ray Magnetic Circular Dichroism Sum Rules for Iron and Cobalt, *Phys. Rev. Lett.* **75**, 152 (1995).
- [30] P. Carra, B. T. Thole, M. Altarelli, and X. Wang, X-Ray Circular Dichroism and Local Magnetic Fields, *Phys. Rev. Lett.* **70**, 694 (1993).
- [31] B. T. Thole, P. Carra, F. Sette, and G. van der Laan, X-Ray Circular Dichroism As a Probe of Orbital Magnetization, *Phys. Rev. Lett.* **68**, 1943 (1992).
- [32] J. Okabayashi, J. W. Koo, H. Sukegawa, S. Mitani, Y. Takagi, and T. Yokoyama, Perpendicular magnetic anisotropy at the interface between ultrathin Fe film and MgO studied by angular-dependent x-ray magnetic circular dichroism, *Appl. Phys. Lett.* **105**, 122408 (2014).
- [33] W. Tang, E. Sanville, and G. Henkelman, A grid-based Bader analysis algorithm without lattice bias, *J. Phys.: Condens. Matter* **21**, 084204 (2009).
- [34] K. Momma and F. Izumi, VESTA 3 for three-dimensional visualization of crystal, volumetric and morphology data, *J. Appl. Crystallogr.* **44**, 1272 (2011).